MIT Libraries | DSpace@MIT

MIT Open Access Articles

The Effects of Charge Motion and Laminar Flame Speed on Late Robust Combustion in a Spark-Ignition Engine

The MIT Faculty has made this article openly available. ***Please share*** how this access benefits you. Your story matters.

Citation: Wildman, Craig, and Wai K. Cheng. "The Effects of Charge Motion and Laminar Flame Speed on Late Robust Combustion in a Spark-Ignition Engine." SAE International Journal of Engines 3(1):202-213, 2010.

As Published: http://dx.doi.org/10.4271/2010-01-0350

Publisher: SAE International

Persistent URL: http://hdl.handle.net/1721.1/66904

Version: Author's final manuscript: final author's manuscript post peer review, without publisher's formatting or copy editing

Terms of use: Creative Commons Attribution-Noncommercial-Share Alike 3.0

Massachusetts Institute of Technology

The Effects of Charge Motion and Laminar Flame Speed on Late Robust Combustion in a Spark-Ignition Engine

Craig B. Wildman and Wai K. Cheng
Sloan Automotive Laboratory, Massachusetts Institute of Technology

Copyright © 2010 SAE International

ABSTRACT

The effects of charge motion and laminar flame speeds on combustion and exhaust temperature have been studied by using an air jet in the intake flow to produce an adjustable swirl or tumble motion, and by replacing the nitrogen in the intake air by argon or CO_2, thereby increasing or decreasing the laminar flame speed. The objective is to examine the "Late Robust Combustion" concept: whether there are opportunities for producing a high exhaust temperature using retarded combustion to facilitate catalyst warm-up, while at the same time, keeping an acceptable cycle-to-cycle torque variation as measured by the coefficient of variation (COV) of the net indicated mean effective pressure (NIMEP). The operating condition of interest is at the fast idle period of a cold start with engine speed at 1400 RPM and NIMEP at 2.6 bar. A fast burn could be produced by appropriate charge motion. The combustion phasing is primarily a function of the spark timing. At each spark timing, however, there is an optimal charge motion that could minimize the COV of NIMEP while not substantially changing the end of combustion (measured by the 90% burn location: CA90). The exhaust temperature is only a function of CA90, irrespective of whether the CA90 is changed by spark timing, charge motion, or laminar flame speed. By using an appropriate amount of charge motion, the exhaust temperature could be raised by 100^{o} C while keeping the same COV of NIMEP.

INTRODUCTION

To meet the emissions regulatory requirements, it is essential to after-treat the spark-ignition engine exhaust with a catalyst. The treatment, however, is not effective before the catalyst reaches a light-off temperature (~300°C). Consequently, a major portion of the total emissions produced in the Federal Test Procedure (FTP-75) occurs during the first tens of seconds of engine operation before the catalyst reaches light-off temperature [1]. The hydrocarbon (HC) emissions during this period are especially severe because the cold environment is not favorable for the mixture preparation process. Enabling the catalyst to light off quickly will substantially reduce overall HC emissions.

One strategy to accomplish fast catalyst light-off is to increase the exhaust enthalpy flow by retarding the spark timing [2]. Then combustion occurs substantially late in the expansion stroke, and less work is extracted by the piston. Late combustion also results in a lower heat loss by the charge because the peak temperature is lower and the burned gas has less residence time in the cylinder. These factors contribute to a hotter exhaust. Furthermore, to provide the same torque output, a higher through put rate is required to compensate for the unfavorable combustion phasing, thereby increasing the exhaust sensible enthalpy flow. Retarding combustion

also directly decreases HC emissions due to the hotter post-flame oxidation environment encountered by the unburned HC in the late expansion and exhaust processes [3, 4].

Retarding combustion phasing has the undesirable effect of substantially increasing the cycle-by-cycle variations (CCV) in torque. When combustion is substantially retarded from maximum brake torque (MBT) timing, the torque is much more sensitive to the heat release schedule and CCV goes up accordingly. Furthermore, since the local turbulence level plays a strong role in determining the burn rate, and since the origin of much of the charge motion and turbulence is in the intake process, when combustion is late, there is a much longer elapse time for the turbulence to develop before it affects the flame. Since turbulent flow is a chaotic process, a longer development time would lead to a higher level of cycle-to-cycle variation. Thus a fast-burn/slow-burn combustion system usually has a higher/lower CCV in torque. The CCV is especially severe under idle condition. At the low idle speed, the elapse time between intake and combustion is longer so that there is a larger cycle-to-cycle variation in the local fluid motion. The low manifold pressure and low speed result in a low Reynolds number, thus the intake process is not effective at generating high turbulence. Also, the residual gas fraction is high. These factors contribute to a slow burn combustion system and thus a high CCV. The factors affecting CCV are: variations in charge motion; variations in the mixture inhomogeneity in temperature and concentration; variations in the amounts of the reactants; variations in the spark discharge. Charge motion effects appear to play the dominant role [5].

Increasing CCV in torque worsens the noise-vibrations-harshness (NVH) quality of the engine. Increasing combustion phasing CCV leads to driveability and emissions problem because some of the cycles may be so late that there are partial burn and misfired cycles. Thus two confounding effects have to be balanced in managing the cold start process: the combustion should be sufficiently retarded to provide a high exhaust enthalpy flow for catalyst fast light-off, but should be not so retarded to avoid high CCV in torque. Therefore, an engine design with a “Late Robust Combustion” is most desirable.

In this study, we assess the effects of charge motion and laminar flame speed on combustion phasing and CCV in torque. A variable-flow air jet in the intake port is used to create various degree of in-cylinder charge motion. Then the nitrogen of the air supply is substituted with carbon dioxide or argon to decrease or increase the laminar flame speed respectively. Relationships between burn duration, combustion phasing, exhaust gas temperature, and coefficient of variation (COV) of net indicated mean effective pressure (NIMEP) are explored. The objective is to find the factors that would promote late robust combustion.

FLAME PROPAGATION AND CHARGE MOTION

The spark ignition engine flame propagation process is reviewed here in the context of the experiment. It has been well established [2] that the spark ignition process initiates a small flame kernel which propagates first in a laminar manner with a smooth flame front. After the kernel grows to be larger than the characteristic turbulent eddy length scale, the flame propagation process is controlled by the fluid turbulence through the wrinkling of the flame front. The latter process can be described by a simple entrainment-and-burn model suggested by Keck [6, 2]. The flame front, with nominal frontal area of A_f takes in unburned gas of density ρ_u with an entrainment velocity u_t which is equal to the local turbulent velocity fluctuation. This entrained gas is then consumed in a time scale given by ℓ_t / S_L where ℓ_t is the turbulent length scale and S_L is the laminar flame speed.

$$\frac{d\mu}{dt} = \rho_u A_f u_t - \frac{\mu}{\ell_t / S_L} \quad (1)$$

In Eq.(1), μ is the mass of unburned gas which is entrained but not burned yet. Then the mass burn rate $\dot{m}_b$ is the sum of the laminar burning at the nominal front and that of the entrained unburned mixture.

$$\frac{dm_b}{dt} = \rho_u A_f S_L + \frac{\mu}{\ell_t / S_L} \quad (2)$$

From Eq. (1) and (2), the quasi-steady (i.e. when $\frac{d\mu}{dt} = 0$) burn rate is:

$$\frac{dm_b}{dt} = \rho_u A_f (S_L + u_t) \quad (3)$$

The quasi-steady burning velocity is, therefore, S_L+u_t. Thus the turbulent velocity augments the laminar flame speed after the flame front transforms from a smooth surface to a wrinkle one. Under conditions for which the laminar speed is too low, however, the burn-out time ℓ_t / S_L will be comparable or longer than the diffusion time $\ell_t{}^2/D$, (where D is the mass diffusivity), and the wrinkle laminar flame model will no longer be valid. Then the combustion progresses slowly in a distributed manner.

The relationship between charge motion and the local turbulence that enhances flame propagation is not straight forward [7]. Only the small eddies are effective in wrinkling the flame front. It has been established that the small scale turbulence generated in the intake process are mostly dissipated in the compression process. The turbulence that matters is produced by the breakup of organized charge motion such as the swirl and tumble motion generated by the induction process. Thus the break up details substantially affects the burn rate.

EXPERIMENTAL SET UP

A 1.8L I-4 DOHC spark-ignition engine was modified for single cylinder operation on a motoring dynamometer. See Table 1 for the engine specifications. The engine features a centrally located spark plug, a shallow bowl-in-piston, and it is representative of modern spark-ignition engines. The intake and exhaust systems were modified to separate the flow through one cylinder from the other three.

Table 1. Engine Specifications

Displacement	442.3cm3
Compression Ratio	9.5
Bore	80mm
Stroke	88mm
Clearance Volume	52cm^3
Connecting Rod Length	140.5mm

A Kistler 6051A piezoelectric pressure transducer coupled to a Kistler 5010 charge amplifier was used for in-cylinder pressure measurements. In-cylinder pressure was pegged to the Manifold Absolute Pressure (MAP) at BDC of the intake stroke. Air flow was measured directly with a 505-9A-02 Kurz flow meter. Fuel flow was calculated based on the equivalence ratio, as measured in the exhaust by an Etas Lambda Meter. Intake air temperature, coolant temperature, and exhaust temperature were recorded. The latter value was measured by a bare thermocouple (type K) approximately 20 cm from the exhaust valve. No radiation correction was applied.

CHARGE MOTION PRODUCING JET

An air jet was installed in the intake port to produce charge motion. (The original charge motion control plate in the intake port was removed.) A nozzle, made out of a copper tube with an inside diameter of 4.8mm, was supplied by a pressurized bottle of air. The mass flow rate of the resulting jet was controlled by a pressure regulator and a choked flow orifice of known diameter that was changed for different ranges of flow rates. The fraction of total intake air that was supplied by the air jet in the charge motion tests was varied from 0 to 1 by changing the jet flow and by adjusting the intake air throttle valve. The nozzle was mounted through the fuel injector hole in the port so that the end of the tube was positioned just behind one of the intake valves. (See later section for fuel introduction.) It was directed in two orientations to generate swirl motion or tumble motion respectively as shown in Fig 1.

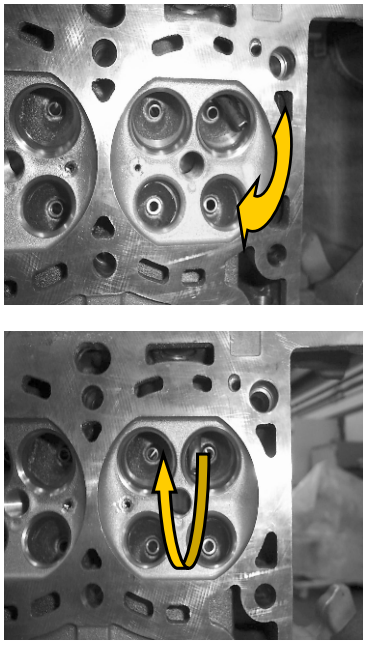

Fig. 1 Charge Motion Producing Jets. Each jet was installed immediately behind an intake valve to generate swirl (top photograph) or tumble (bottom photograph) respectively.

CHANGING THE LAMINAR FLAME SPEED

The composition of the non-reactive gas in the intake air was varied in two sets of tests to study the effects of laminar flame speed on burn duration and COV of IMEP. In the first set, the intake flow consisted of air augmented by a mixture of O2 and argon so that effectively, the nitrogen in the air was substituted with argon in various amounts. Because of the higher specific heat ratio of argon, the laminar flame speed was enhanced. In a second set, CO2 was used instead of argon to decrease laminar flame speed. The air augmentations were introduced far up-stream in the intake system so that the base engine charge motion was not affected.

OPERATING CONDITIONS AND ANALYSIS

Operating conditions were controlled to simulate a fast-idle state shortly after engine start. Speed was held constant at 1400 rpm, and the engine coolant temperature was kept at 20˚C with an industrial chiller. All tests were conducted at $\lambda = 1$ and at 2.6 bar NIMEP. The spark timing was varied from 20˚ BTC to 20˚ ATC in 5˚

increments. Since the experiments were conducted at constant NIMEP, higher MAP was required to compensate for the loss of indicated efficiency with the retarded combustion.

Gaseous propane was used for fuel instead of gasoline to eliminate the possibility of CCV of fuel vaporization. Initially, the propane was introduced into the intake manifold by a nozzle. However, under the condition when most of the air was supplied by the charge motion producing jet, there was inadequate air/fuel mixing; then variations in λ significantly increased and manifest as substantial torque fluctuation. To address this issue, a fuel tube was installed to direct fuel into the port next to the air tube. Then the fuel was introduced into the high speed air jet and rapid fuel/air mixing was achieved.

Data were collected for 300 cycles for statistical analysis. Heat release for each cycle was calculated using the Rassweiler and Withrow method [8].

RESULTS

It is difficult to characterize the details of the charge motion produced by the air jets. Instead, the results are parameterized by the amount of air introduced by the jet as fraction of the total air. The corresponding tumble and swirl numbers are estimated from the jet flow rate and geometry of the jet; see Appendix A.

CHARGE MOTION EFFECTS ON COMBUSTION

The effects of the tumble flow produced by the air jet on the 0-10% burn duration (early part of the flame development) and 10-90% burn duration (major heat release process) are shown in Fig. 2 as a function of the normalized jet flow for the different spark timings. Both burn durations increased when the combustion phasing was retarded. As the jet flow increased, both burn durations were shortened. The faster burn may be attributed to the increase in local turbulence level due to the air jet.

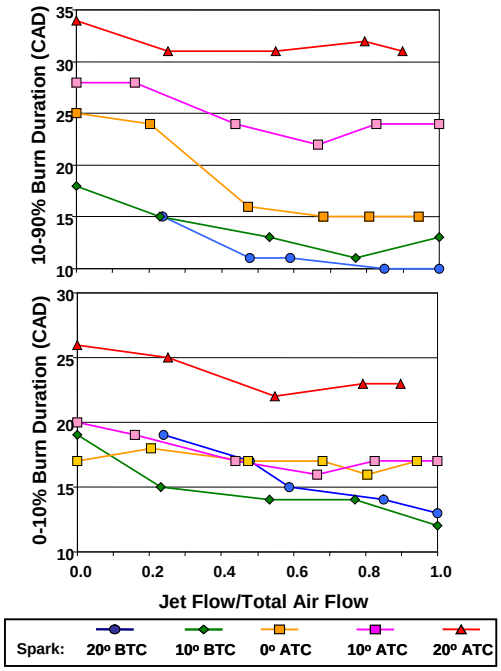

Fig. 2 The 0-10% and 10-90% burned durations for tumble flow; as function of the fraction of total air flow in the jet, and at different spark timings.

The effects of the tumble flow on the COV of NIMEP are shown in Fig. 3. At each spark timing, the COV first decreases and then increases with the increase of the jet flow. This trend is more evident in Fig. 4, in which the COV of NIMEP is plotted against the location at which 90% of the total fuel is burned (CA90). In this figure, the data points are segregated in groups according to the spark timing. In each group, the points are connected in the order of increasing jet flow. For the base line case (with no air jet flow), COV increases with the increase of CA90 produced by the spark retard. However, at each spark timing, there is an optimal charge motion that could reduce the COV values without significantly changing the CA90 values.

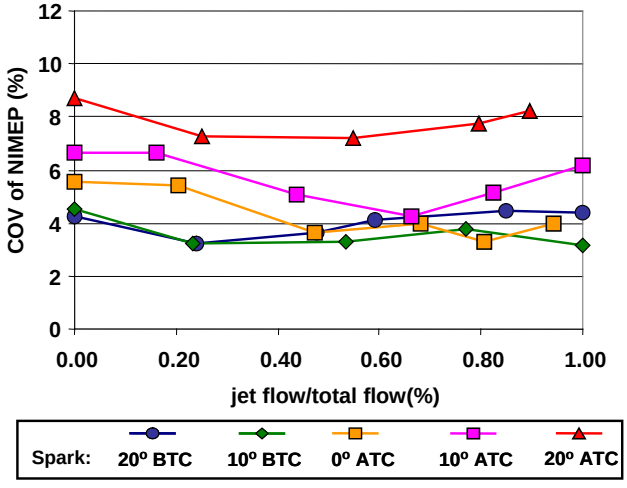

Fig. 3 The COV of NIMEP for tumble flow; as function of the fraction of total air flow in the jet, and at different spark timings

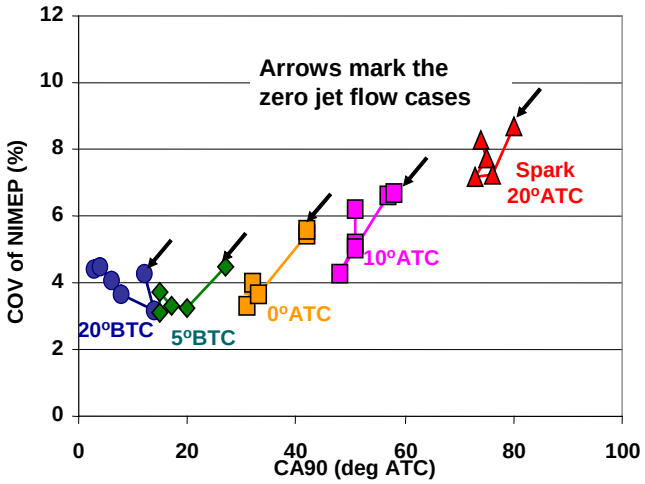

Fig.4 COV of NIMEP as function of CA90 at the different spark timings; tumble flow. Data points connected in the order of increasing jet flow.

For the swirl flow produced by the air jet, the burn durations and COV of IMEP as a function of the jet flow are shown in Figures 5 and 6. Both the 0-10% and 10-90% burn durations, and the COV of NIMEP decreased with the increase of the jet flow at first because of the flame propagation enhancement by the turbulence produced by the swirl. When the jet flow is more than approximately 50% of the total air flow, however, there is no definite dependence on the jet flow rate. Because no measurement has been done on the detailed charge motion, this behavior could not be easily explained.

The COV of NIMEP is plotted against CA90 for the swirl case in Fig. 7. The data are again segregated according to the spark timing. The results are similar to the tumble case (see Fig. 4) – at each spark timing, there is an optimal swirl that would lower the COV without substantially changing the CA90 values.

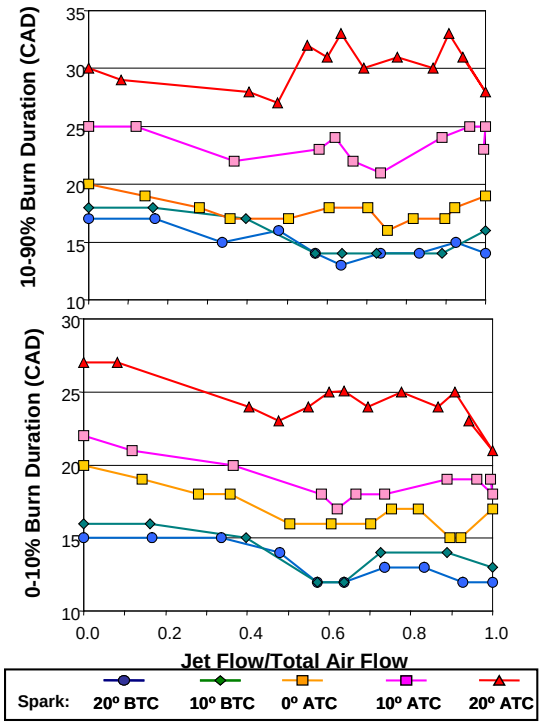

Fig. 5 The 0-10% and 10-90% burned duration for swirl flow versus the fraction of total air flow in the jet

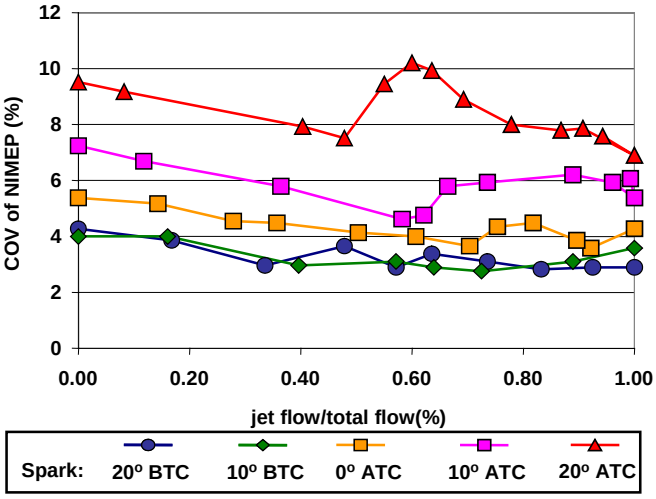

Fig. 6 The COV of NIMEP for swirl flow; as function of the fraction of total air flow in the jet

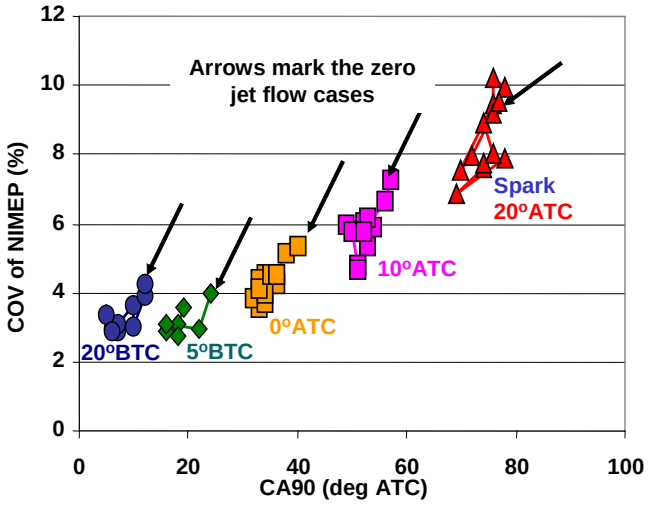

Fig.7 COV of NIMEP as a function of CA90 at the different spark timings; swirl flow. Data points connected in the order of increasing jet flow.

FLAME SPEED EFFECTS ON COMBUSTION

When the nitrogen in air is substituted by argon or CO_2, the laminar flame speed of the resulting mixture is determined by first finding its adiabatic flame temperature, T_{adia}. (The residual gas was not included in this calculation.) Then the relative laminar flame speed is given by the empirical correlation [9]:

$$\frac{S_L}{S_{L,0}} = 1 - 2.52 \left(1 - \frac{T_{adia}}{T_{adia,0}}\right)^{0.684} \quad (4)$$

In this expression, the terms with subscript 0 refer to the properties when the mixture comprises fuel and air only (i.e. no CO_2 or argon replacement of N_2).

The 0-10% and 10-90% burn durations are plotted versus the relative laminar flame speed S_L/S_{L0} in Fig. 8. Both burn durations decrease when the relative laminar flame speed is increased from 1 with the argon substitution. When the relative laminar speed is decreased from 1 with the CO_2 substitution, the durations first increased along the same trend line as the argon substitution. When S_L/S_{L0} was less than approximately 0.85, however, the burn durations increase rapidly. This behavior indicates a transition of the combustion from a wrinkled laminar flame regime to a distributed combustion regime.

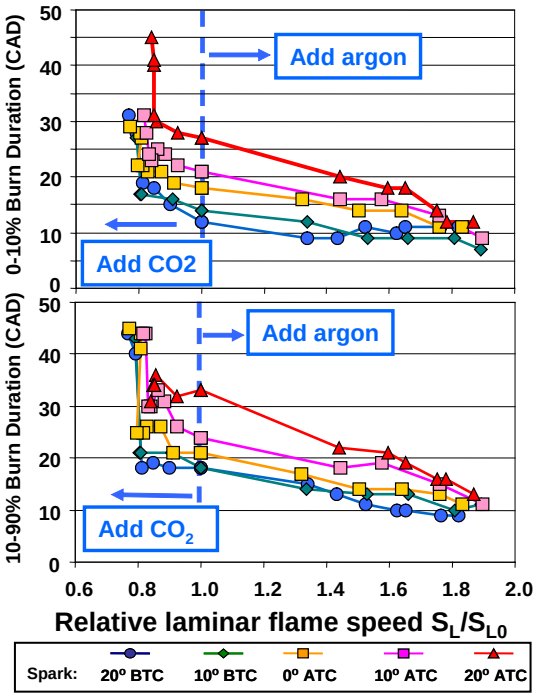

Fig.8 The 0-10% and 10-90% burn durations as a function of relative laminar flame speed.

The COV of IMEP as a function of the relative laminar flame speed at different spark timings is shown in Fig. 9. When S_L/S_{L0} is larger than 1, the COV values are not sensitive to the laminar flame speed for early spark timing (spark before TDC). For spark timing at TDC or after, the COV values decrease first when S_L/S_{L0} is increased from 1; when the S_L/S_{L0} value is larger than 1.4, however, the COV is not sensitive to the flame speed.

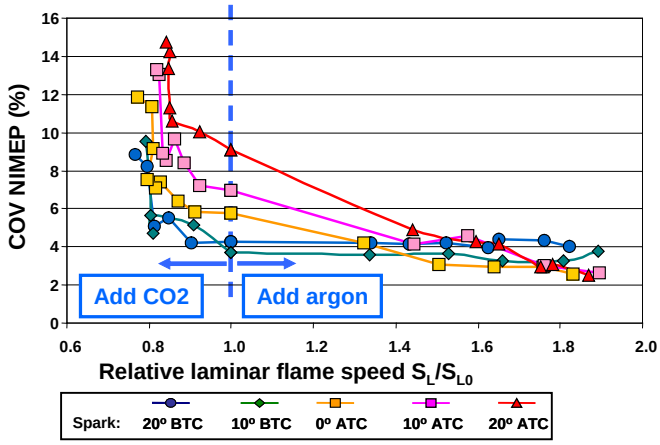

Fig. 9 COV of NIMEP as a function of relative laminar flame speed

When S_L/S_{L0} is decreased from 1, the COV increases modestly at first; when S_L/S_{L0} is less than approximately 0.85, the COV increased rapidly. This behavior is consistent with the transition of combustion from the wrinkled laminar flame to distributed combustion.

COV OF NIMEP VERSUS BURN DURATION

The COV of NIMEP as a function of the 0-10% burn duration is shown in Fig. 10. All the data are included in the plot. For fast initial burn (0-10% duration less than ~15^{o} CA), the COV of NIMEP is not sensitive to the 0-10% burn duration. Then the COV values increase linearly until the 0-10% burn duration reached 30^{o} CA. For the longer burn durations obtained with the CO_2 experiments, the data are much more scattered.

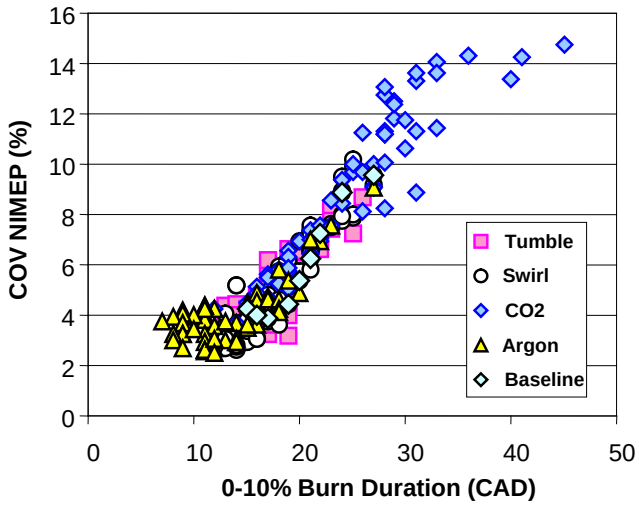

Fig. 10 COV of NIMEP as a function of the 0-10% burn duration. . Data from both charge motion and flame speed variations.

The same trend is observed in the COV of NIMEP versus 10-90% burn duration plot (Fig. 11). Substantial scatter is observed for the data points with a longer 10-90% burn duration. This scatter may be attributed to the transition of the laminar wrinkled flame to the distributed reaction regime of the slow burning cycles. Then the mechanism for the CCV would be changed from depending primarily on charge motion to depending more on the non-uniformity in charge temperature and composition.

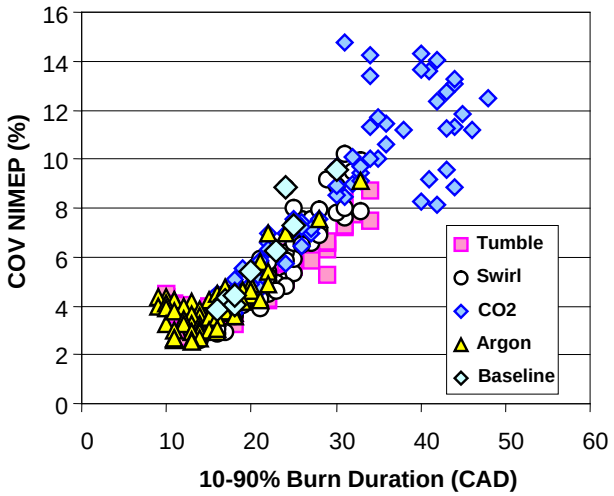

Fig. 11 COV of NIMEP as a function of the 10-90% burn duration. Data from both charge motion and flame speed variations.

EXHAUST TEMPERATURE

As explained in the introduction, the exhaust temperature is primarily related to the combustion phasing – retarded combustion would lead to a higher exhaust temperature. The relationship between exhaust temperature and CA90 is shown in Fig. 12 for all the data. There is good correlation between exhaust temperature and CA90, irrespective of whether the combustion phasing change was generated by change of spark timing, of tumble or swirl motion, or of the laminar flame speed by substituting the nitrogen in the air by argon or CO2. Note that the result was independent of whether the combustion was in the wrinkle laminar flame or distributed combustion regimes. Note also that the effects of the specific heat ratio on the compression and expansion processes and the heat transfer effects almost cancel out the difference in the burned gas temperatures so that the result is not sensitive to the inert gas (N_2, CO_2, and Argon) fraction.

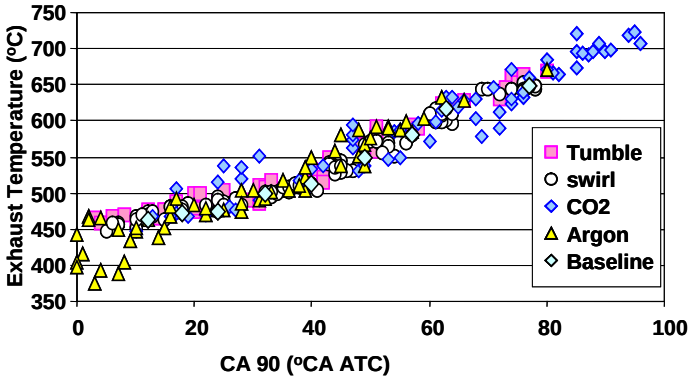

Fig. 12 Exhaust temperature as a function of the 90% mass fraction burn location for the complete data set.

The relationship between the exhaust temperature and the COV of NIMEP is shown in Fig. 13 for the baseline, tumble and swirl charge motion cases for the air data. The general trend was that the exhaust temperature increased with COV of NIMEP, since both quantities increased with retarded combustion. There was, however, differences between the baseline data and those obtained with charge motion – for the same COV of NIMEP, the charge motion produced a higher exhaust temperature. For example, at a COV value of 5%, the exhaust

temperature could increase by 100^{o} C by the appropriate charge motion (going from operating point A to C in Fig. 13). Equivalently, for the same exhaust temperature, the COV values could be lowered by charge motion; For example, at 600^{o} C exhaust temperature, the COV value could be lowered from 8 to 5%. This observation is consistent with the data shown on Figures 4 and 7, that the COV values could be lowered by charge motion while not appreciably changing the CA90, and thus the exhaust temperature. Therefore optimal charge motion could substantially improve the degree of late robust combustion.

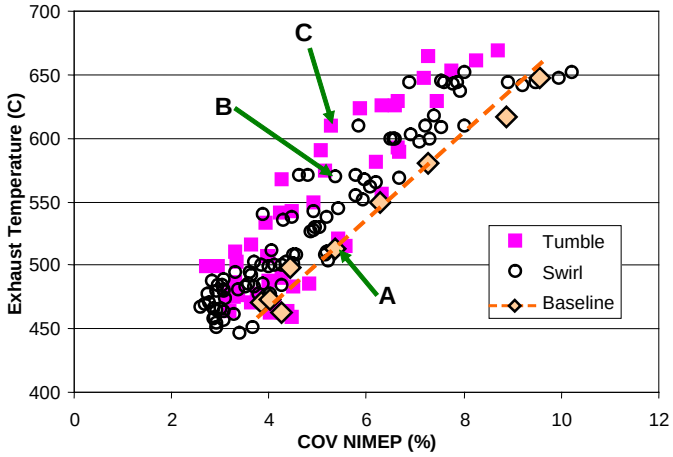

Fig. 13 Exhaust temperature versus the COV of NIMEP; data for the baseline, tumble and swirl cases.

To further understand the mechanism for this improvement, the data points corresponding to the operating points A, B, and C in Fig. 13 were examined in more details. The exhaust temperature and COV of NIMEP are compared in Fig. 14. The exhaust temperature increased by 100^{o} C as CA90 was retarded from 40^{o} to 63^{o} ATC, while the COV of NIMEP decreased marginally.

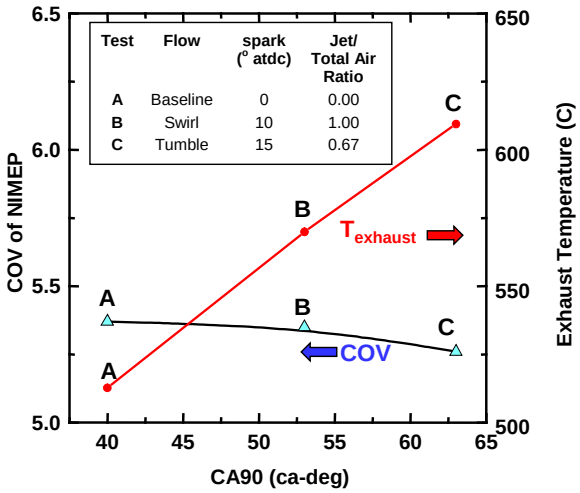

Fig. 14 COV of NIMEP and exhaust temperatures of operating points A, B, and C in Fig. 13.

The progression of the burn curves are shown in Fig. 15. Note that the combustion in case C is substantially retarded because the spark timing was at 15^{o} ATC. As a result, a very late CA90 (at 63^{o} ATC) was achieved.

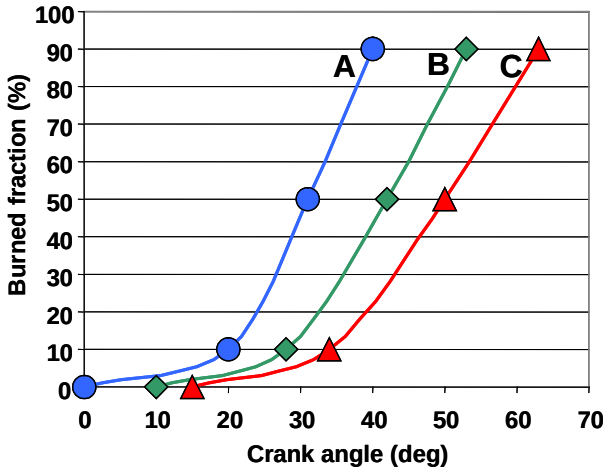

Fig. 15 Burn curves for cases A, B and C in Fig. 13. The spark timings were at 0, 10 and 15o ATC respectively.

When the burn curves are re-plotted as a function of time after spark (Fig. 16), case C had the slowest burn overall. However, the initial parts of the burn curves (up to the 10% burn point) were essentially identical of the three cases. Since it is the initial part of the burning process that is most susceptible to cycle-to-cycle variation [2], the burn curves support the COV data of Fig. 14.

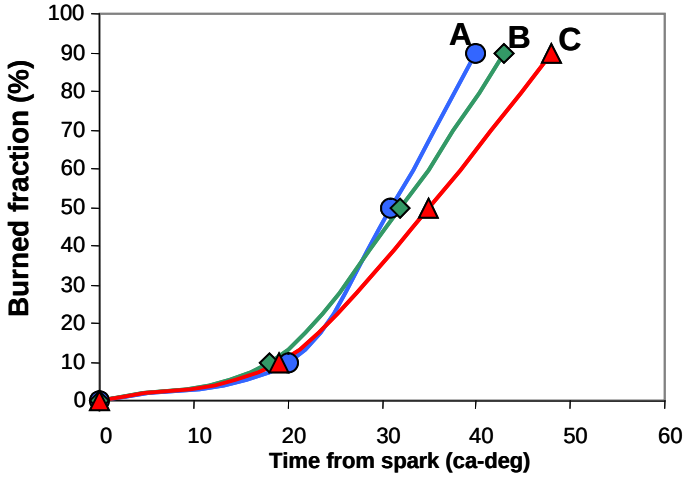

Fig. 16 Burn curves for cases A, B and C; as a function of time from spark.

It should also be noted that combustion started in case C when the piston had substantially descended (at 15^{o} ATC). Thus to maintain the same initial burn (0-10%) rate as in case A, but with a much lower charge temperature and density, the local turbulence level must be substantially higher. However, to obtain a slower overall burn, this turbulence must decay so that the later (10-90%) burn rate slows down. Thus the late robust combustion concept depends much on the control of the engine turbulence.

SUMMARY/CONCLUSIONS

The effects of charge motion and laminar flame speeds on combustion and exhaust temperature have been studied by using an air jet in the intake flow to produce an adjustable swirl or tumble motion, and by replacing the nitrogen in the intake air by argon or CO2, thereby increasing or decreasing the laminar flame speed. The

objective is to examine the "Late Robust Combustion" concept: whether there are opportunities for producing a high exhaust temperature using retarded combustion to facilitate catalyst warm-up, while at the same time, keeping an acceptable COV of NIMEP. The results for an engine operating at fast idle (1400 rpm, 2.6 bar NIMEP) are summarized as follows.

1. Faster burn (both for the 0-10% and 10-90% burn durations) could be achieved by induced charge motion.
2. The COV of NIMEP is not simply related to the intensity of the induced charge motion. At each spark timing, there is an optimum charge motion for the lowest COV value.
3. Increasing the laminar speed resulted in faster 0-10% and 10-90% burn durations. When the relative laminar speed (referenced to the fuel air mixture value) is reduced to 0.85 or lower, the burn durations and the COV of NIMEP increases rapidly, indicating a transition from the laminar wrinkled flame to the distributed reaction regime.
4. For fast burned cycles (with both 0-10%, and 10-90% burn durations less than ~15^{o} CA) the COV of NIMEP is not sensitive to burn duration.
5. For slower cycles (with both 0-10%, and 10-90% burn durations between ~15 to 30^{o} CA) the COV of NIMEP varies approximately linearly with the burn durations.
6. For the very slow cycles (with both 0-10%, and 10-90% burn durations longer than ~30^{o} CA), there is no definite relationship between the COV values and burn durations. These data correspond to the experiments with low laminar flame speed produced by replacing nitrogen with CO_2. The data reflect the transition of combustion from the wrinkled laminar to the distributed reaction regime.
7. The exhaust temperature is only a function of the CA90 value irrespective of the manner the combustion phasing was achieved: by change in spark timing, in charge motion or in laminar flame speed.
8. By optimizing the charge motion, the COV of NIMEP may be held the same while the exhaust temperature could be increased by ~100^{o} C.

Thus appropriate charge motion control could produce late robust combustion. It is desirable to have a fast initial (0-10%) burn rate, but a slower later (10-90%) burn rate. Thus the late robust combustion concept depends on the control of the engine turbulence: In particular, the breakup process of the large scale motion such as swirl and tumble into the small scale turbulence which is responsible for flame propagation.

REFERENCES

1. Eastwood, Peter, *Critical Topics in Exhaust Gas Aftertreatment*. Research Studies Press Ltd., Baldock, Hertfordshire, England, 2000.
2. Heywood, John B., *Internal Combustion Engine Fundamentals*. McGraw-Hill, Inc., New York, NY, 1988.
3. Russ, S., Thiel, M., and Lavoie, G. "SI Engine Operation with Retarded Ignition: Part 2-HC Emissions and Oxidation," SAE paper 1999-01-3507, 1999.
4. Hallgren, B. and Heywood, J. "Effects of Substantial Spark Retard on SI Engine Combustion and Hydrocarbon Emissions," SAE paper 2003-01-3237, 2003.
5. Hinze, P.C. and Cheng, W.K. "Assessing the Factors Affecting SI Engine Cycle-to-Cycle Variations at Idle," Twenty-Seventh Symposium on Combustion, The Combustion Institute, pp. 2119-2126, 1998.
6. Beretta, G.P., Rashidi, M., and Keck, J.C. "Turbulent Flame Propagation and Combustion in Spark Ignition Engines," Combustion and Flame. Vol. 52. pp. 217-245, 1983.
7. Hill, P.G., and Zhang, D., "The Effects of Swirl and Tumble on Combustion in Spark Ignition Engines," Prog. in Energy Cumbust. Sci. Vol. 20, pp. 373-429, 1994.
8. Rassweiler, G. M. and Withrow, L. "Motion Pictures of Engine Flames Correlated with Pressure Cards," SAE Transactions., Vol. 83, pp. 185-204, 1938.

9. Rhodes, D.B. and Keck, J.C. “Laminar Burning Speed Measurements of Indolene-Air-Diluent Mixtures at High Pressures and Temperature,” SAE paper 850047, 1985.

CONTACT INFORMATION

Craig B. Wildman, 31-061F, MIT, Cambridge, Massachusetts, USA.; email: craigwildman@gmail.com

Wai K. Cheng, 31-165, MIT, Cambridge, Massachusetts, USA; email: wkcheng@mit.edu

ACKNOWLEDGMENTS

We would like to thank Thane DeWitt and Raymond Phan of the Sloan Automotive Lab for the engine set up. This work was sponsored by the Nissan Motor Company.

DEFINITIONS/ABBREVIATIONS

a	Distance of charge motion producing jet to the axis of rotation of charge motion
A_f	Nominal flame frontal area
ATC	After-Top-Center
BTC	Before-Top-Center
CA90	Crank angle of 90% mass fraction burned
CCV	Cycle-to-Cycle Variation
COV	Coefficient of Variation
FTP	Federal Test Procedure
H	Angular momentum of charge
HC	Hydrocarbon
λ_t	Turbulent length scale
m	Injected mass for producing charge motion
m_b	Burned mass
M	Total charge mass
MAP	Manifold Absolute Pressure
MBT	Maximum Brake Torque
NIMEP	Net Indicated Mean Effective Pressure

R	Radius
RPM	Revolution per minute
S_L	Laminar flame speed
$S_{L,0}$	Reference laminar flame speed
t	time
T_{adia}	Adiabatic flame temperature
$T_{adia,0}$	Reference adiabatic flame temperature
u	Tangential component of jet velocity
u_t	Turbulent velocity fluctuation
λ	Air/fuel equivalence ratio
μ	Entrained mass that is not yet burned
Ω	Equivalent angular velocity of charge mass
ρ_u	Unburned gas density

APPENDIX

SWIRL AND TUMBLE NUMBER OF CHARGE MOTION

The details of the charge motion created by the jet flows were not measured. The gross motion, however, could be described by a swirl or tumble number estimated according to the jet flow. For a charge mass M contained within a radius R and rotating as a solid body rotation with angular velocity of Ω, the total angular momentum H of the charge is:

$$H = \frac{\Omega R^2}{2} M \quad \text{(A1)}$$

For the jet flow creating the swirl, if the component of the jet velocity tangential to the liner is u and the distance of the jet from the cylinder axis is a, the angular momentum H_t trapped in the cylinder is:

$$H_t = \int (\dot{m}\, ua)dt = mua \quad \text{(A2)}$$

where m is the injected mass. The swirl number is obtained by finding the equivalent of Ω by equating (A1) and (A2), and then normalizing Ω by the engine rotating speed:

$$\text{Swirl No.} = \frac{8ua}{B^2} \frac{m}{M} \frac{60}{2\pi\, RPM} \quad \text{(A3)}$$

Here R is replaced by B/2 where B is the bore.

For the jet flow creating the tumble, the definition is similar, but with the axis of rotation at the mid stroke. Thus

$$\text{Tumble No.} = \frac{8ua}{L^2}\frac{m}{M}\frac{60}{2\pi\ \text{RPM}} \quad \text{(A4)}$$

Here, R is replaced by L/2, where L is the stroke. The Tumble numbers and the Swirl numbers for the jet flows are shown in Figures A1 and A2.